FULL PAPER

Engineering the Magnetic Dipolar Interactions in 3D Binary Supracrystals Via Mesoscale Alloying

*Zhijie Yang, Jingjing Wei, Pierre Bonville, and Marie-Paule Pileni**

Inspired by metallic alloys in atomic solids, two distinct metallic nanoparticles are used, considered as "artificial metal atoms," to engineer ordered binary nanoparticle alloys at the mesoscale, called binary supracrystals. Here, ferromagnetic 7.2 nm Co nanoparticles are used as large "A" site particles, while either ferromagnetic 4.6 nm Co or nonmagnetic 4.0 nm Ag nanoparticles are used as small "B" site particles to fabricate long-range ordered binary supracrystals with a stoichiometry of AB_2 and AB_{13}. The interparticle distances between 7.2 nm Co nanoparticles within the Co/Ag binary supracrystals can be tuned by a control of crystal structure from AB_2 ($CoAg_2$) to AB_{13} ($CoAg_{13}$). A decrease of magnetic coupling between Co nanoparticles is observed as the Co–Co interparticle distance increases. Furthermore, by alloying 7.2 and 4.6 nm Co nanoparticles to form AB_2 ($CoCo_2$) binary supracrystals, a collective magnetic behavior of these two particle types, due to the dipolar interaction, is evidenced by observing a single peak in the zero-field-cooled magnetization curve. Compared with the $CoAg_2$ binary supracrystals, a spin orientation effect in sublattice that reduces the dipolar interactions in the supracrystals is uncovered in $CoCo_2$ binary supracrystals.

1. Introduction

Colloidal crystallization is an efficient way of producing ordered 3D supracrystals in which magnetic, plasmonic, and semiconductor nanoparticles are in close contact. Hence, collective physical properties of these ordered materials are expected to occur because of the dipolar and quantum mechanical interactions between the nanoparticles.[1–8] Indeed, as a result of periodic ordering of the nanoparticles, these 3D supracrystals exhibit unique transport, optical, and structural collective properties.[7–9] Binary supracrystals coassembled from two distinct nanoparticles provide the potential to design these "artificial solids" with programmable chemical and structural features.[10] During the last decade, extensive studies on the self-assembly and structure analysis of binary system have been conducted.[5,10–21] Unfortunately, less effort has been devoted to studies on the collective physical properties of these new materials.[22–25] For example, synergism in binary system exerting enhanced *p*-type conductivity in self-assembled PbTe/Ag_2Te thin films was reported, and these assemblies show markedly enhanced conductance with respect to the sum of individual conductance of single component PbTe and Ag_2Te films.[23] Furthermore, improved thermal stability and catalyst with engineered metal-oxide contacts in binary systems were demonstrated very recently.[24,25]

Ferromagnetic nanoparticles have a magnetic moment that can either rotate randomly between well-defined crystallographic directions, namely the easy magnetic axes[26], or be blocked along these easy axes, depending on the temperature. In a magnetic nanoparticle system where nanoparticles are small enough to have a single magnetic domain, each nanoparticle acts like a "super" spin. Thus in a magnetic nanoparticle superlattice, nanoparticles tend to align their magnetic moments in the direction of the local magnetic field due to the neighboring nanoparticles, called magnetic dipolar interactions.[27] Collective magnetic dipolar interactions were also demonstrated to be present in binary systems made of magnetic nanoparticles with two sizes, as a result of single-phase magnetic behavior, and this effect was found to be present in various systems, such as Fe_3O_4–Fe_3O_4 and Fe_3O_4–FePt.[28] However, the role of small magnetic nanoparticles within magnetic binary supracrystals in the collective magnetic coupling is still unclear and needs to be further unveiled.

In this manuscript, 3D binary supracrystals with stoichiometry AB_2 and AB_{13} were produced using 7.2 nm Co nanoparticles as large "A site" particles, and either 4.6 nm Co or 4.0 nm Ag nanoparticles as small "B site" particles. For simplicity, $CoAg_2$, $CoCo_2$, and $CoCo_{13}$ are used to denote the structure of the binary supracrystals, where the molar ratio between the small and large nanoparticles is given. DC susceptibility measurements were carried out to assess the magnetic properties of these binary assemblies, revealing the effect of mesoscale alloying on the magnetic coupling of supracrystals.

Dr. Z. Yang, J. Wei, Prof. M.-P. Pileni
Sorbonne Universités
UPMC Univ Paris 06, UMR 8233, MONARIS
F-75005 Paris, France
E-mail: mppileni@orange.fr
Dr. Z. Yang, J. Wei, Prof. M.-P. Pileni
CNRS, UMR 8233, MONARIS
F-75005 Paris, France
Dr. P. Bonville, Prof. M.-P. Pileni
CEA/IRAMIS, CEA Saclay
F-91191 Gif-sur-Yvette, France

DOI: 10.1002/adfm.201501499

2. Results and Discussion

Two different sized amorphous Co nanoparticles (7.2 and 4.6 nm) along with polycrystalline 4.0 nm Ag nanoparticles were used as building blocks to engineer the growth of binary assemblies (transmission electron microscopy (TEM) images of the nanoparticles can be found in the Supporting Information). The as-prepared nanoparticles are dispersed in toluene. Each colloidal solution in which either Co or Ag nanoparticles are dispersed is set to the same nanoparticle concentration (5.8×10^{-7} M). The binary system was produced by controlling the relative amount of Co and Ag nanoparticles.[29] A silicon wafer or a TEM grid covered by carbon films was placed at the bottom of a beaker in which 200 µL or 40 µL respectively of the mixed colloidal solution was injected. The solvent was then evaporated very slowly to permit the nanoparticles to self-assemble into 3D ordered assemblies.

Because the soft coatings on the nanoparticles have no trivial effect on the nanoparticle assembly, the nanoparticle effective diameter (d_{eff}), defined as the nanoparticle center-to-center distance in a self-ordered compact hexagonal network, has to be taken into account. It was determined from the corresponding TEM images.[29] The effective diameters of Co nanoparticles with an average diameter of 4.6 and 7.2 nm with 10% and 9% as size dispersion (Figure S1, Supporting Information) are 7.7 ± 0.8 nm and 10.2 ± 1.1 nm, respectively, whereas the effective diameter of 4.0 nm Ag nanoparticles is 6.0 ± 0.5 nm.

Let us first consider Co/Ag binary systems with a relative concentration ratio of [Co]/[Ag] = 1/2. **Figure 1** shows the TEM images of $CoAg_2$ superlattices with AlB_2-type binary structure. The $CoAg_2$ structure consists of hexagonally ordered large Co nanoparticles, together with the smaller Ag nanoparticles inserted into the vacancies between the Co layers, which agrees well with the literature with AlB_2 structure (space group P6/mmm).[30] Three sets of typical crystal superlattice planes are observed: (001) (Figure 1a), (110) (Figure 1c), and (100) (Figure 1e) superlattice planes, and the corresponding projections of the model structures can be found in Figure 1b,d,f, respectively. The superlattice spacings in the (100) and (001) planes measured from the corresponding TEM images are 10.4 and 12.0 nm, corresponding to lattice dimensions $a = b =$ 12.1 nm and $c = 12.0$ nm. The center-to-center distance between Co nanoparticles in $CoAg_2$ superlattices was calculated for these various orientations: the average distance between Co nanoparticles is 12.0 ± 0.2 nm and the edge-to-edge value (δ) between Co nanoparticles is estimated to be 4.8 ± 0.2 nm. This value markedly differs from that in single-component *fcc*-phase Co superlattices (3.4 nm) (data shown in Supporting Information). The domain size of the $CoAg_2$ binary supracrystals is up to tens of micrometers as observed previously.[29]

Let us now consider $CoCo_2$ binary systems produced from two colloidal solutions one containing 4.6 nm and the other 7.2 nm Co nanoparticles. The concentration of each colloidal solution is the same as above (5.8×10^{-7} M). According to the relative nanoparticles' size ratio, $\gamma_{eff} = 0.76 \pm 0.02$, $MgZn_2$-type structure is most favorable based on the recent theoretical work shown that the $MgZn_2$ phase to be stable in the size ratio range of $0.76 \leq \gamma \leq 0.84$.[20] Here, by careful analysis

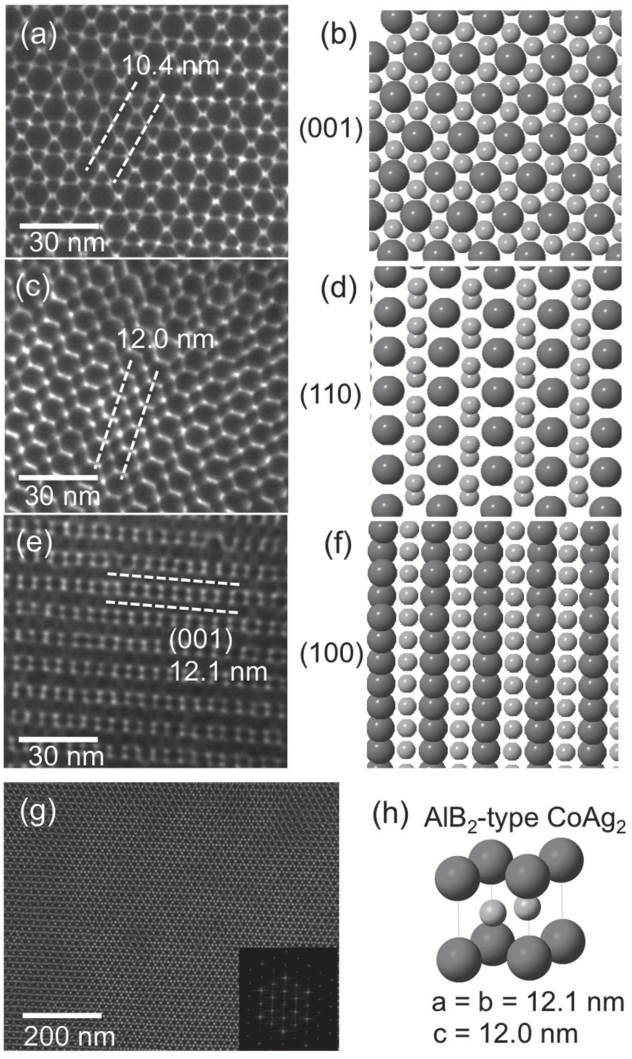

Figure 1. TEM images of $CoAg_2$ binary nanoparticle superlattices with various crystal planes: a,b) (001) plane; c,d) (110) plane; e,f) (100) plane; g) low magnification of (001) plane; h) crystal model of AlB_2 structure. Inset in panel (g) is the corresponding FFT pattern.

of the TEM data, we only observe an AB_2 binary structure isostructural with that of $MgZn_2$ (Space Group $P6_3/mmc$) for this radius ratio (**Figure 2**). The structure of $MgZn_2$ contains four molecular units per unit cell with the smaller Zn atoms ordered in tetrahedra, whereas the larger Mg atoms fall into the vacancies provided by the Zn tetrahedral (shown in Figure 2h). Typical TEM images of these structures with the (001) plane parallel to the substrate are shown in Figure 2a,b and the corresponding structure model projected along the same zone axis in Figure 2c. The FFT pattern in the inset of Figure 2a shows the hexagonal symmetry. From this set of crystal planes, it is possible to evaluate the unit cell length $a = b = 16.9 \pm 0.2$ nm. Another crystal plane with indices (210), with a minor fraction parallel to the substrate, is shown in Figure 2d,e, along with the projection of the model structure in Figure 2f. The unit cell edge length measured from this image is $c = 30.1 \pm 0.2$ nm. Thus a unit cell with cell parameters of $a = b = 16.9$ nm and $c =$ 30.1 nm was built to evaluate the various Co–Co interparticle

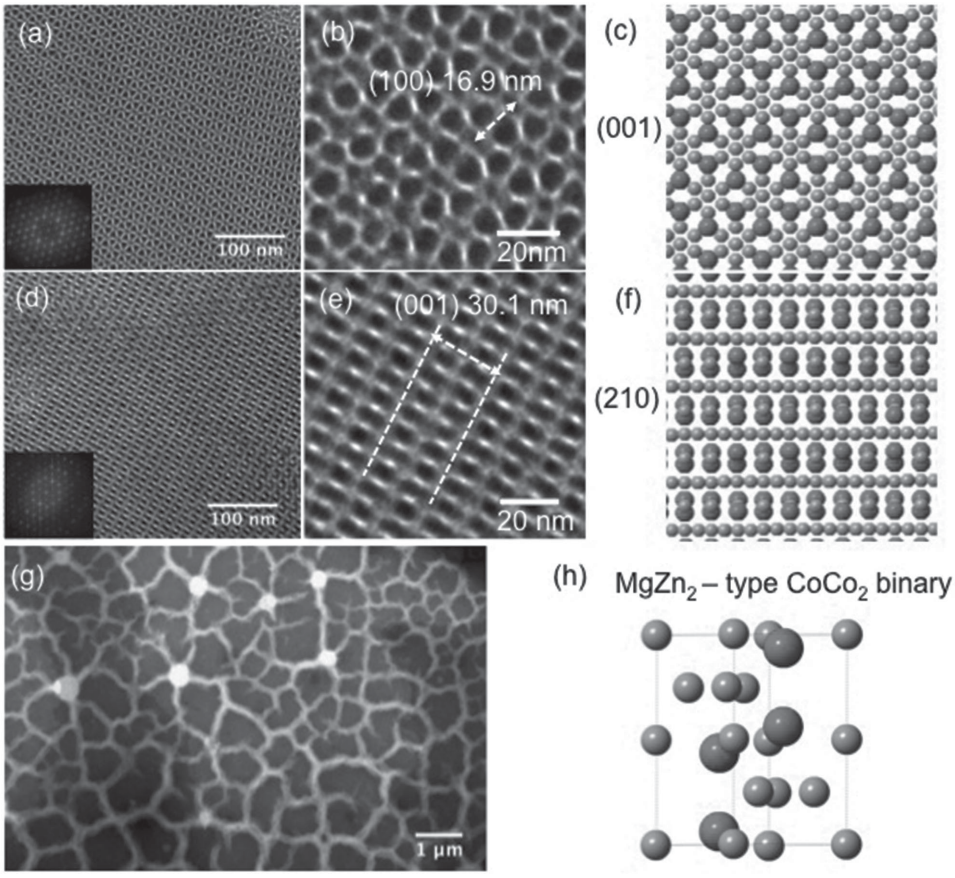

Figure 2. TEM image of binary supracrystals from the evaporation of 7.2 and 4.6 nm Co binary nanoparticle mixtures: a–c) (00l) crystal planes; d–f) (210) crystal planes; g) low magnification shows the cracked films; h) structural model of $MgZn_2$ alloys. Insets in panels (a,d) are the corresponding FFT patterns.

distances (Figure 2h): the nearest gap between 7.2 nm Co nanoparticles is 4.2 ± 0.4 nm, resulting in a Co–Co interparticle distance of 11.4 nm. The domain size of the $CoCo_2$ binary supracrystals is up to ≈5 micrometers.

By increasing the amount of the initial mixed colloidal solution to 200 mL instead of 40 mL and using the same procedures as described above, thick film binary systems of either $CoAg_2$ or $CoCo_2$ were deposited on a silicon wafer (3 mm × 5 mm). The high-resolution scanning electron microscopy (HRSEM) studies of the $CoAg_2$ films further reveal the hexagonally stacking, where each Co nanoparticle is surrounded by six Ag nanoparticles (**Figure 3**). In first approximation, it is assumed that the interparticle distance between large Co (7.2 nm) nanoparticles, determined for thin films, remains similar to that observed for thick 3D supracrystals as already observed previously.[31]

The low field DC magnetic susceptibility of $CoAg_2$ and $CoCo_2$ binary supracrystals described above, and those of single component Co nanoparticles (7.2 and 4.6 nm), shows a behavior typical for an ensemble of size distributed superparamagnetic particles. The zero-field-cooled (ZFC) and field-cooled (FC) magnetization curves were measured in the presence of a 10 G applied magnetic field of 10 Oe. The position of the observed peak in the ZFC curve corresponds to the average magnetic blocking temperature (T_b) of the nanoparticles. Below the T_b, the magnetocrystalline anisotropy energy and dipolar magnetic interaction dominate over the thermal energy k_BT and each particle magnetization is "blocked" (along its individual easy anisotropy axis) with respect to the characteristic time $\tau\chi$ of the measurement (100 s for SQUID magnetometry). Above T_b, the thermal energy is sufficient to allow the particle magnetic moments to depart from their anisotropy axis and to fluctuate: the particles become superparamagnetic. Various positions for the ZFC peak can be observed on the curves.

Figure 4a shows the ZFC/FC magnetization curves of both 4.6 and 7.2 nm *fcc* Co supracrystals characterized by an interparticle distance, deduced from grazing-incidence small angle X-ray scattering, of 3.2 and 3.4 nm (Supporting Information). The blocking temperature T_b is 185 and 50 K, respectively, for the 7.2 and 4.6 nm supracrystals. An approximate expression for the blocking temperature is

$$k_BT_b = E_a/\mathrm{In}\left(\tau_\chi/\tau_0\right) \quad (1)$$

where $E_a = K_{eff}V$, K_{eff} being the effective anisotropy energy density and V the nanoparticle volume,[32] and τ_0 a microscopic time of the order of 10^{-10} s. Hence, the higher T_b for the larger sized Co nanoparticle supracrystals is due to the larger nanoparticle volume implying a larger magnetocrystalline anisotropy

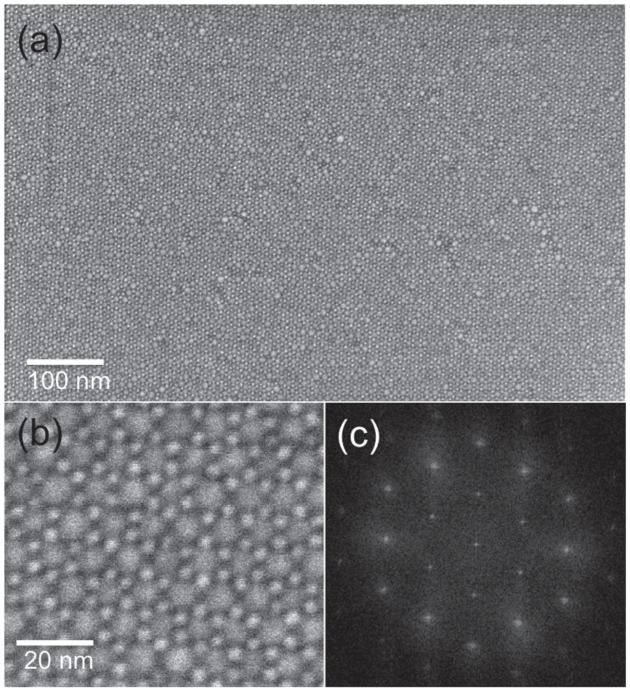

Figure 3. High-resolution SEM images of AlB_2-type $CoAg_2$ 3D binary supracrystals: a) low-magnification image; b) high-magnification image; c) FFT pattern taken from panel (a).

energy. The FC curve of 7.2 nm Co supracrystals shows a slight decrease below 185 K (T_b), indicating a spin-glass like behavior, while for 4.6 nm Co supracrystals the FC curves show a monotonic increase below the corresponding T_b with a saturating trend at sufficiently low temperatures, indicating relatively weaker interparticle coupling interactions between the nanoparticles.[33,34]

The blocking temperatures of $CoAg_2$ and $CoCo_2$, deduced from the ZFC/FC curves, are 166 and 121 K, respectively (Figure 4b). Note that for $CoCo_2$, where two different sized Co nanoparticles are present, a single peak is observed for the ZFC curve, and the T_b (121 K) is intermediate between the T_bs of supracrystals with a single Co component (4.6 and 7.2 nm). Furthermore, like for 4.6 nm and contrary to 7.2 nm Co one component supracrystals, the FC curve for $CoCo_2$ shows a monotonic increase below T_b, indicating relatively weaker interparticle interactions. The ZFC peak shifts from 185 K for 7.2 nm Co supracrystals to 166 K for $CoAg_2$ and 121 K for $CoCo_2$ binary supracrystals, respectively (Figure 4a,b). In strongly interacting superparamagnetic particle systems, the blocking temperature may be increased by the coupling between nanoparticles [35] because the dipole–dipole interaction can be considered as an extra energy barrier adding to the anisotropy energy, which consequently hinders thermal fluctuations of the spins. The energy of the dipole–dipole interaction between two magnetic moments μ_i and μ_j, separated by a distance $r_{i,j}$, can be written as[36,37]

$$E_D^{(i,j)} = \frac{\mu_0}{4\pi}\left[\frac{\mu_i \times \mu_j}{r_{i,j}^3} - \frac{3(\mu_i \times r_{ij})(\mu_j \times r_{ij})}{r_{i,j}^5}\right] \quad (2)$$

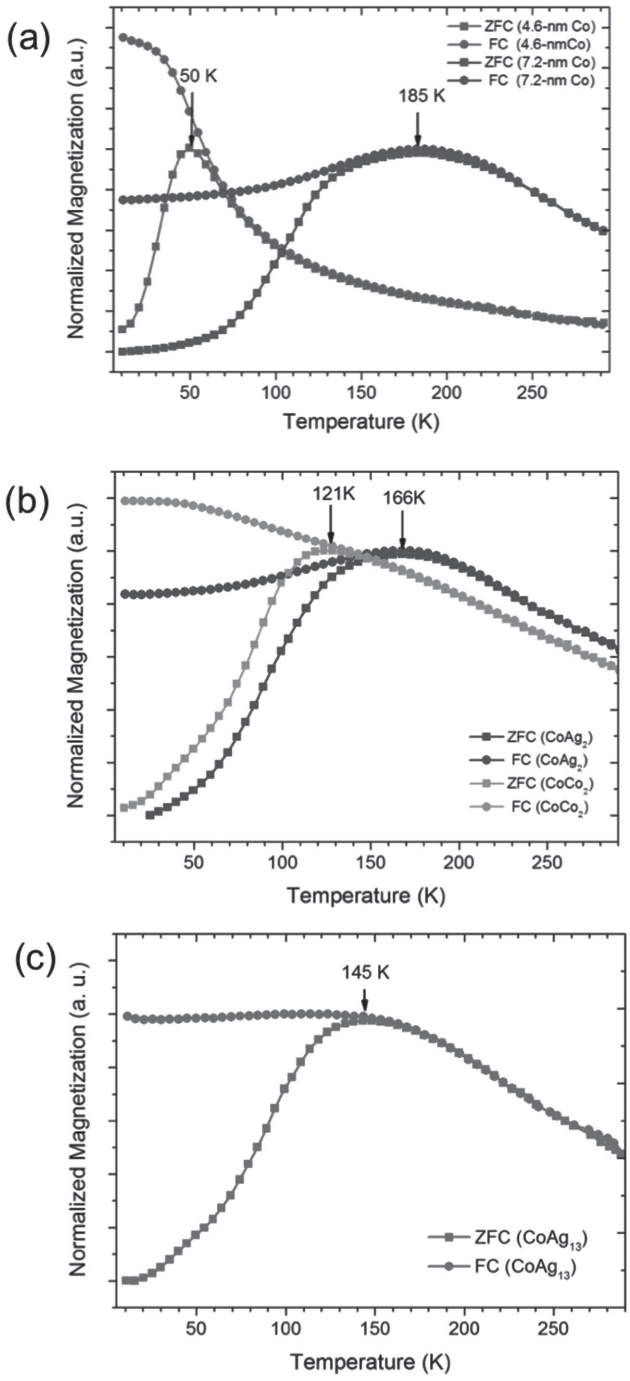

Figure 4. a) Zero-field-cooled (ZFC) and field-cooled (FC) magnetization versus temperature curves measured at 10 G for the 7.2 nm Co supracrystals (purple) and 4.6 nm Co supracrystals (green). b) ZFC/FC magnetization versus temperature curves for two types of AB_2 binary supracrystals, $CoCo_2$ (orange) and $CoAg_2$ (blue) binary supracrystals. c) ZFC/FC magnetization versus temperature curves for $CoAg_{13}$ supracrystals (red).

Our measurements clearly show that, due to their nonmagnetic behavior, Ag nanoparticles act as a spacer to tune the interparticle distance $r_{i,j}$. Hence the dipolar coupling between Co nanoparticles controls, as expected, the magnetic properties of the supracrystals through modulation of the interparticle

Table 1. Structural parameters of various samples for DC susceptibility measurement

Parameters	7.2 nm Co	$CoAg_2$	$CoAg_{13}$	$CoCo_2$
Co–Co [nm]	10.6	12.0	16.1	11.4
Effective filling factor	74%	76%	72%	65%
Co (7.2 nm) Filling factor	23.3%	12.9%	4.7%	10.5%
T_b [K]	185	166	145	121

distance from 10.4 to 16.1 nm, by insertion of Ag nanoparticles. Furthermore, the FC curves for all three samples (Co, $CoAg_2$, and $CoAg_{13}$) show a slight decrease below their corresponding T_b, indicative of a superspin glass behavior as reported for 8 nm Co nanocrystal supracrystals.[38]

Inspection of the average distances for the two binary systems of AB_2 type differing by their structures ($MgZn_2$-type for $CoCo_2$ and AlB_2 for $CoAg_2$) shows that the interparticle distance between 7.2 nm Co in these systems is larger than that determined for the single component 7.2 nm Co supracrystals (see **Table 1**). This could explain the decrease in the blocking temperature of binary systems compared to single component supracrystals. However, the T_b of $CoCo_2$ binary supracrystals is smaller than that of $CoAg_2$ ones (Figure 4b). Here, the interparticle distance cannot be the major factor controlling the T_b value (through the dipole–dipole interaction) because these two binary supracrystals have close Co–Co interparticle distances. Moreover, the change in the effective Co (7.2 nm) filling factor cannot be the factor inducing a drastic decrease in the T_b value (see Table 1). The major difference between these two binary systems lies in the fact that the small nanoparticles are magnetic or not. Here we propose that other parameters such as the coexistence of two magnetic sublattices with different nanoparticle size can affect the magnitude and symmetry of the magnetic energy barriers and reduce the blocking temperature of the system. For $CoCo_2$ binary supracrystals, the energy of the magnetic dipolar interactions can be described as

$$E_D^{(i,j)} = E_D^{(A,A)} + E_D^{(A,B)} + E_D^{B,B} \quad (3)$$

where $E_D^{(A,A)}$, $E_D^{(A,B)}$, and $E_D^{B,B}$ are the magnetic dipolar interactions between various neighboring magnetic nanoparticles, Co(7.2nm)–Co(7.2nm),Co(7.2nm)–Co(4.6nm), and Co(4.6 nm)–Co(4.6 nm), respectively. Due to the larger magnetocrystalline anisotropy energy for Co(7.2 nm) with respect to Co(4.6 nm) nanoparticles, the magnetic moments of Co(4.6 nm) nanoparticles can be pinned by the dipolar field arising from Co(7.2 nm) nanoparticles along a direction quite different from that of the Co(7.2 nm) magnetic moment (see **Scheme 1**). Indeed, for instance, the dipolar field at a point in the plane perpendicular to a given moment is opposite to that moment. This additional dipolar interaction $E_D^{(A,B)}$ between Co(4.6 nm) and Co(7.2 nm) magnetic moments can then contribute to lower the effective anisotropy barrier with respect to that in $CoAg_2$ supracrystals.

To support such a claim let us consider another binary system having a large Co–Co interparticle distance with the lower effective Co (7.2 nm) filling factor. This can be realized by increasing the relative amount of colloidal Ag nanoparticles with respect to the Co one ([Co]/[Ag] = 1/10) while keeping the total nanoparticle concentration constant to 5.8×10^{-7} M, as used previously for the various systems studied. A long-range ordered binary system characterized by $CoAg_{13}$ structure, analogous to molecular solids of icosahedral AB_{13} ($NaZn_{13}$), is then obtained. We shall see that its blocking temperature is still larger than that of $CoCo_2$.

Figure 5 shows the preferential crystal orientation with the (100) plane parallel to the substrate (Figure 5a,b) for the $CoAg_{13}$ supracrystals. In addition, the (110) plane parallel to the substrate shown in Figure 5c further confirms the $NaZn_{13}$-type $CoAg_{13}$ structures.[39] The domain size of $CoAg_{13}$ binary supracrystals is measured to be up to ≈10 micrometers.[29] The $NaZn_{13}$ structure (Space Group *Fm*3*c*) consists of 8 Co nanoparticles and 104 Ag nanoparticles in a unit cell in which the Co nanoparticles are well isolated by several Ag nanoparticles (Figure 5f). The spacings between Co nanoparticles within the binary structure in the (001) and (110) planes are 16.1 ± 0.2 and 12.3 ± 0.2 nm, respectively. The center-to-center distance between Co nanoparticles is calculated to be ≈16.1 nm, thus a large edge-to-edge δ value between Co nanoparticles of ≈8.9 nm was obtained. Similarly as above, by increasing the amount of colloidal solution, a thick film was produced. The HRSEM image in **Figure 6**a shows that the large Co nanoparticles are ordered in a square pattern, which can be verified by the corresponding FFT pattern in Figure 6b. From these data, it is possible to deduce the average distance between Co nanoparticles (summarized in Table 1).

Figure 4c shows the ZFC/FC magnetization curves of $CoAg_{13}$ binary supracrystals. The blocking temperature is 145 K and the FC curve shows a slight decrease below T_b, indicative of constraint as a superspin glass behavior. Note that the blocking

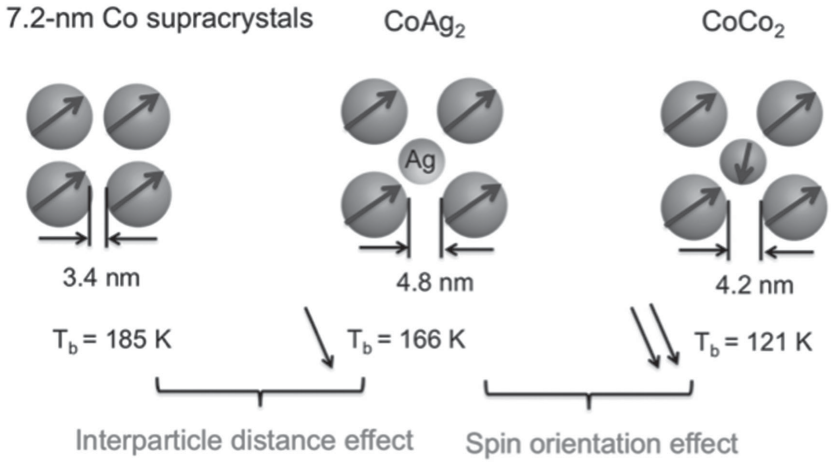

Scheme 1. The influence of the small nanoparticles on the magnetic properties of Co supracrystals.

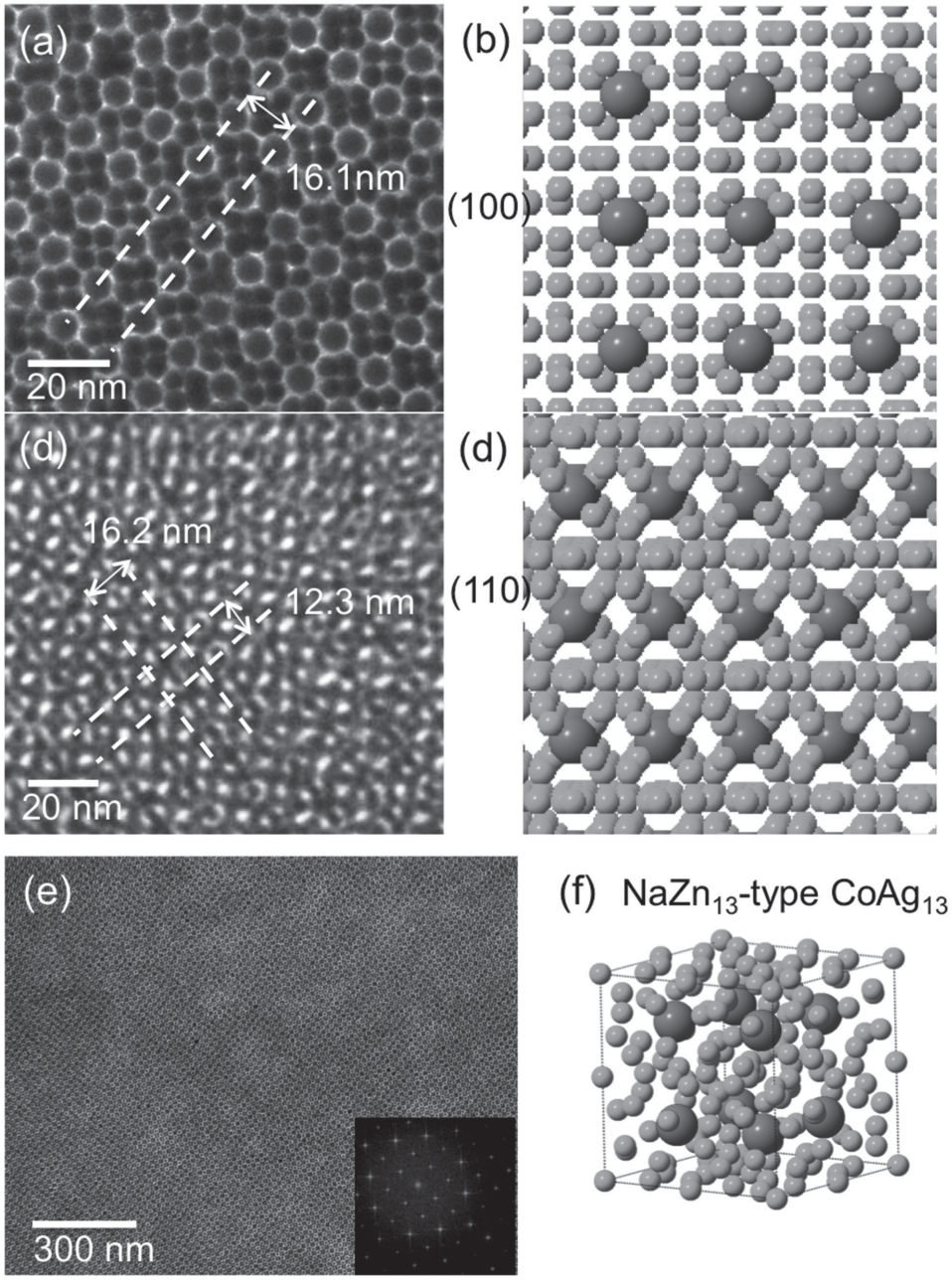

Figure 5. TEM images of $CoAg_{13}$ binary nanoparticle superlattices with various crystal planes: a,b) (001) plane; c,d) (110) plane; e) low magnification of (100) plane; f) crystal model of $NaZn_{13}$ structure. Inset in panel (e) is the corresponding FFT pattern.

temperature of $CoAg_{13}$ supracrystals is higher than that of $CoCo_2$ binary supracrystals (121 K) whereas the interparticle distance between large (7.2 nm) Co nanoparticles is smaller (Table 1). The rather low blocking temperature and the smooth increase in the FC curve on decreasing temperature observed with $CoCo_2$ supracrystals clearly indicate a decrease in the magnetic interactions compared to binary systems produced with nonmagnetic small (Ag) associated with large Co nanoparticles. Hence, $CoCo_2$ supracrystals are characterized by weaker dipolar interactions than their counterpart as $CoAg_2$ and $CoAg_{13}$ supracrystals.

3. Conclusions

In summary, long-range ordered Co nanoparticle based supracrystals, namely single component 7.2 nm Co and binary supracrystals, such as $CoAg_2$, $CoAg_{13}$, and $CoCo_2$ have been produced. These 3D binary supracrystals are considered as mesoscale alloys by inserting small nanoparticles (4.6 nm Co or 4.0 nm Ag) into 7.2 nm Co nanoparticle 3D supracrystals. The magnetic dipolar interactions in 7.2 nm Co supracrystals are tunable by engineering the Co–Co interparticle distance with the formation of Co/Ag binary supracrystals. For the $NaZn_{13}$-type

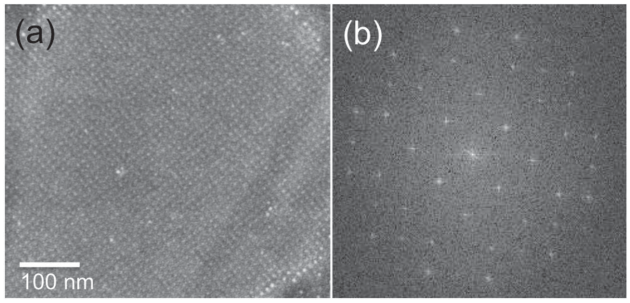

Figure 6. High-resolution SEM images of $NaZn_{13}$-type $CoAg_{13}$ 3D binary nanoparticle supracrystals: a) HRSEM image; b) FFT pattern taken from panel (a).

$CoAg_{13}$ binary supracrystals, a larger interparticle distance between Co nanoparticles results in a reduced dipolar interactions, leading to a lower blocking temperature of the sample. Furthermore, a decrease in the blocking temperature was observed for $CoCo_2$ binary supracrystals, when the nonmagnetic Ag nanoparticles were replaced by magnetic 4.6 nm Co nanoparticles. This suggests that in the $CoCo_2$ binary supracrystals, the spin directions between the large and small Co nanoparticles are different, which reduces the dipolar interactions in the system.

4. Experimental Sections

Chemicals: All materials were used without further purification: cobalt acetate, silver nitrate, dodecanethiol, dodecanoic acid, sodium borohydride, and octylether were from Aldrich; hydrazine, isooctane, and hexane were from Fluka; and sodium di(ethylhexyl) sulfosuccinate (NaAOT) was from Sigma. The synthesis of Ag(AOT) and $(Co(AOT)_2$ were described previously.

Apparatus: Conventional transmission electron microscopy was performed using a JEOL 1011 microscope at 100 kV. DC magnetic properties of the samples were studied by the means of magnetometry measurements and they were compared with the disordered samples. We performed the magnetometry measurements via a commercial superconducting interference device (SQUID). The measurements were performed under an airless atmosphere, and the magnetizations of the samples were measured as a function of in-plane-applied DC magnetic field and temperature.

Synthesis of Co Nanoparticles: Co nanoparticles were synthesis from reverse micelles, as already described.[40] In brief, reverse micelles of $Co(AOT)_2$ (5×10^{-2} M) in the presence of water molecules such that $w = [H_2O]/[AOT] = 32$ were reduced by sodium borohydride as ($R = [NaBH_4]/[Co(AOT)_2] = 6$). Co nanoparticles were immediately produced and oleic acid (316 µL) was added to coat the nanoparticles. The coated Co nanoparticles were then washed and centrifuged four times with ethanol to remove the AOT surfactant and the black powder obtained was dispersed in toluene. At the end of the synthesis, 7.2 nm Co nanoparticles coated with oleic acid with a ≈9% size distribution were produced. The entire synthesis was carried out in an N_2 glove box using deoxygenated solvents to prevent particle oxidation. By using mixed reverse micelles of $Co(AOT)_2$ (5×10^{-2} M) and Na(AOT) (0.1 M) and by keeping the same procedure as described above, Co nanoparticles characterized by an average diameter and size distribution of 4.6 nm and 9%, respectively, were produced. As already observed amorphous-like nanoparticles were obtained. The size of the nanoparticles remained quite unchanged. In the text, the exact average value of the diameters and size distribution determined through a measure of over 500 nanoparticles were given precisely.

Synthesis of Ag Nanocrystals: The Ag nanocrystals coated with dodecanethiol ($C_{12}H_{25}SH$) were synthesized as described elsewhere from 0.1 M reverse micelles of Ag(AOT).[41] The water content, $w = [H_2O]/[AOT]$, was kept at 2. Hydrazine dispersed in 0.1 M Na(AOT) was added to the mixed micelles. Dodecanethiol used as coating agent was then added to the reverse micelles containing the nanocrystals. To remove the AOT surfactant, ethanol was added to the solution. After four times washing with ethanol, the nanocrystals were characterized by a mean diameter of 4.0 nm with a size distribution of 9% and were redispersed in toluene. The crystalline structure of Ag nanocrystals was mainly polycrystalline with a very small contribution of single domain nanocrystals.

Supracrystals Growth: Self-assembly of binary colloidal solution was carried out in an experimental setup shown in elsewhere published before,[42] and the temperature could be controlled (i.e., 35 °C in the present study). Carbon-coated copper TEM grids were used as the substrate for self-assembly experiments. The grids were placed inside a glass vial with inner diameter of ≈4 mm. Then 40 µL of solution containing a mixture of Co and Ag nanocrystals with the desired particle ratio, keeping the overall particle concentration constant 5.8×10^{-7} M, was injected into the glass vial. For the magnetic measurement, silicon wafer (3×5 mm^2) was applied as substrate for the sample deposition and 200 µL of colloidal mixture was used. Concentrations of the Co nanoparticles were estimated according to our previous report.[43] The solution was evaporated under N_2 atmosphere, avoiding any oxidation of Co nanoparticles.

Supporting Information

Supporting Information is available from the Wiley Online Library or from the author.

Acknowledgements

The research leading to these results was supported by an Advanced Grant of the European Research Council under Grant 267129. Z.Y. and J.W. thank the China Scholarship Council for financial support.

Received: April 14, 2015
Revised: June 11, 2015
Published online: July 3, 2015

[1] G. Singh, H. Chan, A. Baskin, E. Gelman, N. Repnin, P. Kral, R. Klajn, *Science* **2014**, *345*, 1149.
[2] M. P. Boneschanscher, W. H. Evers, J. J. Geuchies, T. Altantzis, B. Goris, F. T. Rabouw, S. A. P. van Rossum, H. S. J. van der Zant, L. D. A. Siebbeles, G. Van Tendeloo, I. Swart, J. Hilhorst, A. V. Petukhov, S. Bals, D. Vanmaekelbergh, *Science* **2014**, *344*, 1377.
[3] T. Wang, J. Q. Zhuang, J. Lynch, O. Chen, Z. L. Wang, X. R. Wang, D. LaMontagne, H. M. Wu, Z. W. Wang, Y. C. Cao, *Science* **2012**, *338*, 358.
[4] Z. Nie, A. Petukhova, E. Kumacheva, *Nat. Nanotechnol.* **2010**, *5*, 15.
[5] E. Klecha, I. Arfaoui, J. Richardi, D. Ingert, M. P. Pileni, *Phys. Chem. Chem. Phys.* **2011**, *13*, 2953
[6] M. P. Pileni, *Adv. Funct. Mater.* **2001**, *11*, 323.
[7] N. Goubet, C. Yan, D. Polli, H. Portalès, I. Arfaoui, G. Cerullo, M.-P. Pileni, *Nano Lett.* **2012**, *13*, 504.
[8] P. Yang, I. Arfaoui, T. Cren, N. Goubet, M.-P. Pileni, *Nano Lett.* **2012**, *12*, 2051.
[9] N. C. Bigall, C. Wilhelm, M. Beoutis, M. Garcia-Hernandez, A. A. Khan, C. Giannini, A. Sanchez-Ferrer, R. Mezzenga, M. E. Materia,

M. A. Garcia, F. Gazeau, A. M. Bittner, L. Manna, T. Pellegrino, *Chem. Mater.* **2013**, *25*, 1055.
[10] F. X. Redl, K. S. Cho, C. B. Murray, S. O'Brien, *Nature* **2003**, *423*, 968.
[11] E. V. Shevchenko, D. V. Talapin, N. A. Kotov, S. O'Brien, C. B. Murray, *Nature* **2006**, *439*, 55.
[12] E. V. Shevchenko, D. V. Talapin, C. B. Murray, S. O'Brien, *J. Am. Chem. Soc.* **2006**, *128*, 3620.
[13] M. A. Kostiainen, P. Hiekkataipale, A. Laiho, V. Lemieux, J. Seitsonen, J. Ruokolainen, P. Ceci, *Nat. Nanotechnol.* **2013**, *8*, 52.
[14] D. V. Talapin, E. V. Shevchenko, M. I. Bodnarchuk, X. Ye, J. Chen, C. B. Murray, *Nature* **2009**, *461*, 964.
[15] D. Vanmaekelbergh, *Nano Today* **2011**, *6*, 419.
[16] Z. Chen, J. Moore, G. Radtke, H. Sirringhaus, S. O'Brien, *J. Am. Chem. Soc.* **2007**, *129*, 15702.
[17] M. P. Boneschanscher, W. H. Evers, W. Qi, J. D. Meeldijk, M. Dijkstra, D. Vanmaekelbergh, *Nano Lett.* **2013**, *13*, 1312.
[18] X. Ye, J. Chen, C. B. Murray, *J. Am. Chem. Soc.* **2011**, *133*, 2613.
[19] M. I. Bodnarchuk, M. V. Kovalenko, W. Heiss, D. V. Talapin, *J. Am. Chem. Soc.* **2010**, *132*, 11967.
[20] W. H. Evers, B. D. Nijs, L. Filion, S. Castillo, M. Dijkstra, D. Vanmaekelbergh, *Nano Lett.* **2010**, *10*, 4235.
[21] Z. Yang;J. WeiP. Bonville, M. P. Pileni, *J. Am. Chem. Soc.* **2015**, *137*, 4487.
[22] X. Ye, J. Chen, B. T. Diroll, C. B. Murray, *Nano Lett.* **2013**, *13*, 1291.
[23] J. J. Urban, D. V. Talapin, E. V. Shevchenko, C. R. Kagan, C. B. Murray, *Nat. Mater.* **2007**, *6*, 115.
[24] Y. Kang, X. Ye, J. Chen, L. Qi, R. E. Diaz, V. Doan-Nguyen, G. Xing, C. R. Kagan, J. Li, R. J. Gorte, E. A. Stach, C. B. Murray, *J. Am. Chem. Soc.* **2013**, *135*, 1499.
[25] Y. Yu, C. A. Bosoy, D.-M. Smilgies, B. A. Korgel, *J. Phys. Chem. Lett.* **2013**, *4*, 3677.
[26] Y.-W. Jun, J.-w. Seo, J. Cheon, *Acc. Chem. Res.* **2008**, *41*, 179.
[27] Y. Lalatonne, J. Richardi, M. P. Pileni, *Nat. Mater.* **2004**, *3*, 121.
[28] J. Chen, A. Dong, J. Cai, X. Ye, Y. Kang, J. M. Kikkawa, C. B. Murray, *Nano Lett.* **2010**, *10*, 5103.
[29] Z. Yang, J. Wei, M. P. Pileni, *Chem. Mater.* **2015**, *27*, 2152.
[30] D. K. Smith, B. Goodfellow, D.-M. Smilgies, B. A. Korgel, *J. Am. Chem. Soc.* **2009**, *131*, 3281.
[31] Y. Nagaoka, O. Chen, Z. Wang, Y. C. Cao, *J. Am. Chem. Soc.* **2012**, *134*, 2868.
[32] Y. W. Jun, J. W. Seo, J. Cheon, *Acc. Chem. Res.* **2008**, *41*, 179.
[33] D. Parker, V. Dupuis, F. Ladieu, J. P. Bouchaud, E. Dubois, R. Perzynski, E. Vincent, *Phys. Rev. B* **2008**, *77*, 104428.
[34] S. Sahoo, O. Petracic, W. Kleemann, S. Stappert, G. Dumpich, P. Nordblad, S. Cardoso, P. P. Freitas, *Appl. Phys. Lett.* **2003**, *82*, 4116.
[35] A. F. Gross, M. R. Diehl, K. C. Beverly, E. K. Richman, S. H. Tolbert, *J. Phys. Chem. B* **2003**, *107*, 5475.
[36] J. García-Otero, M. Porto, J. Rivas, A. Bunde, *Phys. Rev. Lett.* **2000**, *84*, 167.
[37] J. Du, B. Zhang, R. K. Zheng, X. X. Zhang, *Phys. Rev. B* **2007**, *75*, 014415.
[38] D. Parker, I. Lisiecki, M. P. Pileni, *J. Phys. Chem. Lett.* **2010**, *1*, 1139.
[39] E. V. Shevchenko, D. V. Talapin, S. O'Brien, C. B. Murray, *J. Am. Chem. Soc.* **2005**, *127*, 8741.
[40] Z. Yang, N. Yang, J. Yang, J. Bergström, M. P. Pileni, *Adv. Funct. Mater.* **2015**, *25*, 891.
[41] A. Courty, A. Mermet, P. A. Albouy, E. Duval, M. P. Pileni, *Nat. Mater.* **2005**, *4*, 395.
[42] Y. F. Wan, N. Goubet, P. A. Albouy, M. P. Pileni, *Langmuir* **2013**, *29*, 7456.
[43] I. Lisiecki, D. Parker, C. Salzemann, M. P. Pileni, *Chem. Mater.* **2007**, *19*, 4030.